

# Probing real-space and time resolved correlation functions with many-body Ramsey interferometry

Michael Knap,<sup>1,2,\*</sup> Adrian Kantian,<sup>3</sup> Thierry Giamarchi,<sup>3</sup>  
Immanuel Bloch,<sup>4,5</sup> Mikhail D. Lukin,<sup>1</sup> and Eugene Demler<sup>1</sup>

<sup>1</sup>*Department of Physics, Harvard University, Cambridge MA 02138, USA*

<sup>2</sup>*ITAMP, Harvard-Smithsonian Center for Astrophysics, Cambridge, MA 02138, USA*

<sup>3</sup>*DPMC-MaNEP, University of Geneva, 24 Quai Ernest-Ansermet CH-1211 Geneva, Switzerland*

<sup>4</sup>*Max-Planck-Institut für Quantenoptik, Hans-Kopfermann-Str. 1, 85748 Garching, Germany*

<sup>5</sup>*Fakultät für Physik, Ludwig-Maximilians-Universität München, 80799 München, Germany*

(Dated: October 9, 2013)

We propose to use Ramsey interferometry and single-site addressability, available in synthetic matter such as cold atoms or trapped ions, to measure real-space and time resolved spin correlation functions. These correlation functions directly probe the excitations of the system, which makes it possible to characterize the underlying many-body states. Moreover they contain valuable information about phase transitions where they exhibit scale invariance. We also discuss experimental imperfections and show that a spin-echo protocol can be used to cancel slow fluctuations in the magnetic field. We explicitly consider examples of the two-dimensional, antiferromagnetic Heisenberg model and the one-dimensional, long-range transverse field Ising model to illustrate the technique.

PACS numbers: 47.70.Nd, 05.30.-d, 75.10.Jm, 67.85.-d, 37.10.Ty

In condensed matter systems there exists a common framework for understanding such diverse probes as neutron and X-ray scattering, electron energy loss spectroscopy, optical conductivity, scanning tunneling microscopy, and angle resolved photoemission. All of these techniques can be understood in terms of dynamical response functions, which are Fourier transformations of retarded Green's functions [1]

$$G_{\text{ret}}^{AB,\mp}(t) := -\frac{i\theta(t)}{Z} \sum_n e^{-\beta E_n} \langle n|B(t)A(0)\mp A(0)B(t)|n\rangle. \quad (1)$$

Here, the summation goes over all many-body eigenstates  $|n\rangle$ ,  $\beta = 1/k_B T$ , the partition function  $Z = \sum_n e^{-\beta E_n}$ , operators are given in the Heisenberg representation  $A(t) = e^{i\hat{H}t} A e^{-i\hat{H}t}$  ( $\hbar$  is set to one in this manuscript), signs  $-(+)$  correspond to commutator(anticommutator) Green's functions, and  $\theta(t)$  is the Heaviside function. Correlation functions provide a direct probe of many-body excitations and their weight, describe many-body states, and give particularly important information about quantum phase transitions, where they exhibit characteristic scaling forms [2].

In the last few years the experimental realization of many-body systems with ultracold atoms [3], polar molecules [4], and ion chains [5] has opened new directions for exploring quantum dynamics. However, most dynamical studies of such “synthetic matter” correspond to quench or ramp experiments: The initial state is prepared, then it undergoes some nontrivial evolution  $|\Psi(t)\rangle = T_t e^{-i \int_0^t dt' \hat{H}(t')} |\Psi(0)\rangle$  and some observable  $A$  is measured  $\langle A(t) \rangle = \langle \Psi(t) | A | \Psi(t) \rangle$ . These experiments provide an exciting new direction for exploring many-body dynamics, but they do not give direct information

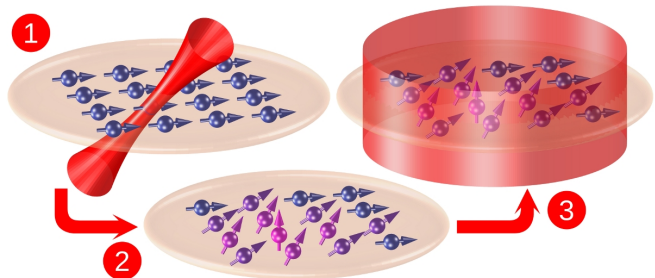


FIG. 1. (Color online) Many-body Ramsey interferometry consists of the following steps: (1) A spin system prepared in its ground state is locally excited by  $\pi/2$  rotation, (2) the system evolves in time, (3) a global  $\pi/2$  rotation is applied, followed by the measurement of the spin state. This protocol provides the dynamic many-body Green's function.

about excitations of many-body systems as contained in dynamical response functions. Notable exceptions are phase or amplitude shaking of the optical lattice (see, e.g., [6–8] and references therein) and radio frequency spectroscopy [9], which can be understood as measuring the single particle spectral function (i.e. the imaginary part of the corresponding response function). However, these techniques can not be extended to measuring other types of correlation functions, such as spin correlation functions in magnetic states as realized in optical lattices or ion chains and are often carried out in a regime far beyond linear response, which would be required to relate the measurement to theory within Kubo formalism [1].

In this paper, we demonstrate that a combination of Ramsey interference experiments and single site addressability available in ultracold atoms and ion chains can be

used to measure *real-space and time resolved spin correlation* functions; see Fig. 1 for an illustration of the protocol. This is in contrast to established condensed matter probes, which generally measure response functions in frequency and wave vector domain. In principle, the two quantities are connected by Fourier transform, but the limited bandwidth of experiments renders a reliable mapping difficult in practice. We further discuss experimental limitations such as slow magnetic field fluctuations and show that global spin echo can be used to cancel these fluctuations.

**Many-body Ramsey interference.**—We consider a spin-1/2 system and introduce Pauli matrices  $\sigma_j^a$  for every site  $j$  with  $a \in \{x, y, z\}$ . At this point we do not make any assumptions on the specific form of the spin Hamiltonian. Examples will be given below. The internal states  $|\downarrow\rangle_z$  and  $|\uparrow\rangle_z$  of a single site  $j$  can be controlled by Rabi pulses which are of the general form [10, 11]

$$R_j(\theta, \phi) = \hat{1} \cos \frac{\theta}{2} + i(\sigma_j^x \cos \phi - \sigma_j^y \sin \phi) \sin \frac{\theta}{2}, \quad (2)$$

where  $\theta = \Omega\tau$  with the Rabi frequency  $\Omega$  and the pulse duration  $\tau$ , and  $\phi$  the phase of the laser field. For the many-body Ramsey interference we consider spin rotations with  $\theta = \pi/2$  but  $\phi$  arbitrary.

The many-body Ramsey protocol consists of four steps, see Fig. 1 for the first three of them: (1) perform a local  $\pi/2$  rotation  $R_i^1 := R_i(\pi/2, \phi_1)$  on site  $i$ , (2) evolve the system in time for a duration  $t$ , (3) perform a global (or local)  $\pi/2$  spin rotation  $R^2 := \prod_j R_j(\pi/2, \phi_2)$ , and (4) measure  $\sigma^z$  on site  $j$ . The final measurement is destructive but can be carried out in parallel on all sites.

The result of this procedure, after repetition over many experimental runs, corresponds to the expectation value

$$M_{ij}(\phi_1, \phi_2, t) = \sum_n \frac{e^{-\beta E_n}}{Z} \langle n | R_i^\dagger(\phi_1) e^{i\hat{H}t} R^\dagger(\phi_2) \sigma_j^z R(\phi_2) e^{-i\hat{H}t} R_i(\phi_1) | n \rangle. \quad (3)$$

With some algebra we obtain [12]

$$M_{ij}(\phi_1, \phi_2, t) = \frac{1}{2} \left( \cos \phi_1 \sin \phi_2 G_{ij}^{xx,-} + \cos \phi_1 \cos \phi_2 G_{ij}^{xy,-} - \sin \phi_1 \sin \phi_2 G_{ij}^{yx,-} - \sin \phi_1 \cos \phi_2 G_{ij}^{yy,-} \right) + \text{terms with odd number of } \sigma^{x,y} \text{ operators}, \quad (4)$$

where  $G_{ij}^{ab,-}$  is the retarded, commutator Green's function defined in Eq. (1) with  $A = \sigma_i^a$  and  $B = \sigma_j^b$ .

In many physically relevant models, terms with odd number of  $\sigma$  operators vanish by symmetry or at least can be removed by an appropriate choice of the phases  $\phi_1$  and  $\phi_2$  of the laser fields. We show below when using these properties that in cases of both the Heisenberg model, Eq. (6), and the long-range, transverse field Ising

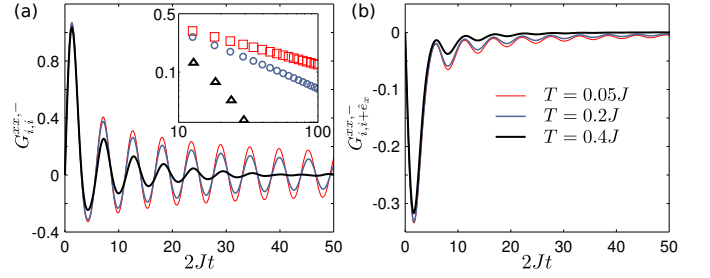


FIG. 2. (Color online) Real-space and time resolved Green's function  $G_{ij}^{xx,-}$  of the two-dimensional, isotropic Heisenberg model, which can be measured with many-body Ramsey interferometry, shown for different temperatures  $T$ . The antiferromagnetic correlations manifest themselves in the opposite phase of on-site (a) and nearest-neighbor (b) correlations. The inset in (a) shows the decay of the peaks in  $G_{ii}^{xx,-}$  on a double logarithmic scale. See main text for details.

model, Eq. (9), our Ramsey interference sequence measures a combination of retarded correlation functions

$$M_{ij}(\phi_1, \phi_2, t) = \frac{1}{4} \left\{ \sin(\phi_1 + \phi_2) (G_{ij}^{xx,-} - G_{ij}^{yy,-}) - \sin(\phi_1 - \phi_2) (G_{ij}^{xx,-} + G_{ij}^{yy,-}) + \cos(\phi_1 + \phi_2) (G_{ij}^{xy,-} + G_{ij}^{yx,-}) + \cos(\phi_1 - \phi_2) (G_{ij}^{xy,-} - G_{ij}^{yx,-}) \right\}. \quad (5)$$

Alternatively to the many-body Ramsey protocol, a spin-shelving technique can be used to measure dynamic spin correlations along the quantization direction, i.e., the operators  $A$  and  $B$  in (1) are  $\sigma_j^z$  and  $\sigma_j^z$ , respectively [12]. In the supplementary material [12] we also derive a useful relation between Green's functions and Loschmidt echo, and discuss that it can be used to characterize diffusive and localized many-body phases.

**Heisenberg model.**—The anisotropic Heisenberg model of the XXZ type, can be realized both with two component mixtures [13–18] and with polar molecules [19–21] in optical lattices

$$\hat{H}_{\text{Heis}} = \sum_{i < j} J_{ij}^\perp (\sigma_i^x \sigma_j^x + \sigma_i^y \sigma_j^y) + J_{ij}^z \sigma_i^z \sigma_j^z. \quad (6)$$

For two component Bose mixtures, interactions can be mediated through the superexchange mechanism and  $J_{ij}^\perp$ ,  $J_{ij}^z$  are functions of the inter- and intra-species scattering lengths which are nonzero for  $i, j$  nearest neighbors. When realizing the Heisenberg model with polar molecules,  $J_{ij}^\perp$ ,  $J_{ij}^z$  are long-ranged and anisotropic in space. Hamiltonian (6) is introduced for arbitrary dimension and the site index  $i$  is understood as a collective index. We assume that the system is prepared in equilibrium at finite temperature, i.e., it has a density matrix given by  $\rho = Z^{-1} e^{-\beta \hat{H}_{\text{Heis}}}$ .

Hamiltonian (6) has the global symmetry  $\sigma^x \rightarrow -\sigma^x$ ,  $\sigma^y \rightarrow -\sigma^y$ , and  $\sigma^z \rightarrow \sigma^z$ , from which it is obvious that expectation values with an odd number of  $\sigma^{x,y}$  vanish. In addition, Hamiltonian (6) has a U(1) symmetry of spin rotations around the  $z$  axis. This symmetry requires that

$$G_{ij}^{xx} - G_{ij}^{yy} = 0 \quad \text{and} \quad G_{ij}^{xy} + G_{ij}^{yx} = 0.$$

Hence, the many-body Ramsey protocol (5) measures

$$M_{ij}(\phi_1, \phi_2, t) = -\frac{1}{4} \left\{ \sin(\phi_1 - \phi_2)(G_{ij}^{xx} + G_{ij}^{yy}) - \cos(\phi_1 - \phi_2)(G_{ij}^{xy} - G_{ij}^{yx}) \right\}. \quad (7)$$

The choice of the phases  $\phi_1$  and  $\phi_2$  of the laser fields, determines which combination of Green's functions is obtained.

In case the two spin states are not encoded in magnetic field insensitive states, one may also need to take into account fluctuating magnetic fields for a realistic measurement scenario. Such a contribution is described by a Zeeman term  $\hat{H}_Z = h_z \sum_i \sigma_i^z$ . A spin-echo sequence, however, which augments the Ramsey protocol with a global  $\pi$  rotation  $R^\pi$  after half of the time evolution, removes slow fluctuations in the Zeeman field

$$\begin{aligned} R(\phi_2) e^{-i(\hat{H}_{\text{Heis}} + \hat{H}_Z) \frac{t}{2}} R^\pi e^{-i(\hat{H}_{\text{Heis}} + \hat{H}_Z) \frac{t}{2}} R_i(\phi_1) \\ \rightarrow \tilde{R}(\phi_2) e^{-i\hat{H}_{\text{Heis}} t} R_i(\phi_1), \end{aligned} \quad (8)$$

where  $\tilde{R}(\phi_2) = iR(\phi_2)(\cos \phi_\pi \prod_l \sigma_l^x - \sin \phi_\pi \prod_l \sigma_l^y)$  and  $\phi_\pi$  the phase of the laser field in the course of the  $\pi$  rotation. We show in [12] that this transformation still allows one to measure dynamic correlation functions.

Figure 2 shows the time-resolved, local (a) and nearest-neighbor (b) Green's function of the antiferromagnetic Heisenberg model ( $J_{ij}^\perp = J_{ij}^z =: J$  for  $i, j \in$  nearest neighbors and  $J_{ij}^\perp = J_{ij}^z = 0$  otherwise) for different temperatures. We obtain the results using a large- $N$  expansion in Schwinger-Boson representation [22–24], which has been demonstrated to give reasonable results for the two-dimensional spin-1/2 Heisenberg antiferromagnet [25]. The local and nearest-neighbor, dynamic Green's functions show clear signatures of antiferromagnetic order, since their oscillations are out of phase. When lowering the temperature, the emergence of quantum coherence manifests through the increase in the amplitude of the oscillations. Further the decay of the oscillations, inset in (a), follows at low temperatures a power-law over several decades in time, which indicates the approach to criticality. The power-law, however, is cut off by the finite correlation time  $\log \tau \sim J/T$ . Dynamic correlations at the antiferromagnetic ordering wave-vector  $\vec{\pi} := (\pi, \pi)$  are a precursor of long-range order [12] which in two dimensions emerges at zero temperature. These correlations can be obtained from the spatial ones by summing up contributions of one sublattice with positive sign and of the other with negative sign.

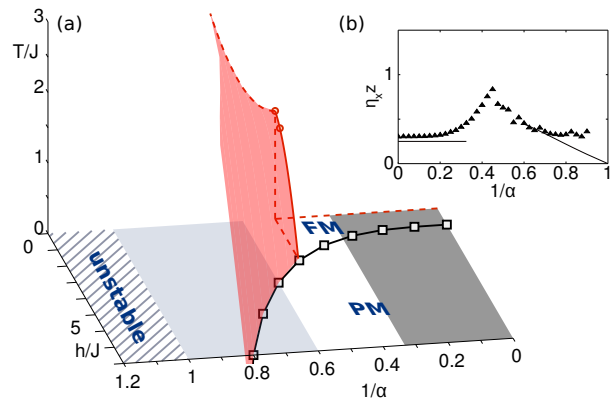


FIG. 3. (Color online) Phase diagram (a) of the one-dimensional, long-range, transverse field Ising model (9) in the transverse field  $h$ , interaction exponent  $\alpha$ , and temperature  $T$  space. For  $\alpha < 1$ , hatched region, the system is thermodynamically unstable. The solid, black line indicates the quantum critical line, which separates the ferromagnetic (FM) and paramagnetic (PM) phase. For  $\alpha > 3$ , dark gray region, the phase transition is of the same universality class as the short-range Ising transition, for  $\alpha < 5/3$ , light gray region, mean-field analysis is exact [12]. At  $\alpha = 2$  and  $h = 0$ , dashed lines, the phase transition is of the Berezinskii-Kosterlitz-Thouless type, which also extends to finite transverse field  $h$  [26]. Symbols which indicate the finite temperature transition correspond to  $h = 0$ ,  $T = 1.5262(5)J$  [27] and  $h = J/2$ ,  $T = 1.42(1)J$  [28]. (b) Critical exponent  $\eta_{xz}$  of dynamic correlations  $G_{L/2, L/2}^{xx, -}(t)$  obtained along the critical line from the scaling of finite size systems, which are realizable in current experiments, symbols, and exact results in the thermodynamic limit, lines.

### Long-range, transverse field Ising model.—

Systems of trapped ions are capable of simulating canonical quantum spin models, where two internal states of the ions serve as effective spin states and the interaction between spins is mediated by collective vibrations [29, 30]. Among the quantum spin models that can be simulated with trapped ions is the long-range, transverse field Ising model

$$\hat{H}_{\text{Ising}} = - \sum_{i < j} J_{ij} \sigma_i^x \sigma_j^x - h \sum_i \sigma_i^y \quad (9)$$

where the spin-spin interactions fall off approximately as a power law  $J_{ij} = J/|i - j|^\alpha$  with exponent  $\alpha$ , and  $h$  is the strength of the transverse field. In trapped ion systems power-law interactions can be engineered with an exponent  $\alpha$  that is highly tunable [29]. The upper limit of  $\alpha$  is given by the decay of dipolar interactions  $0 < \alpha < 3$ , however, the shorter-ranged interactions are, the slower are the overall time scales, which in turn is challenging for experiments.

Experimentally the long-ranged Ising model has been realized with ion chains for both ferromagnetic (FM)  $J > 0$  [31, 32] as well as antiferromagnetic  $J < 0$  [33–39]

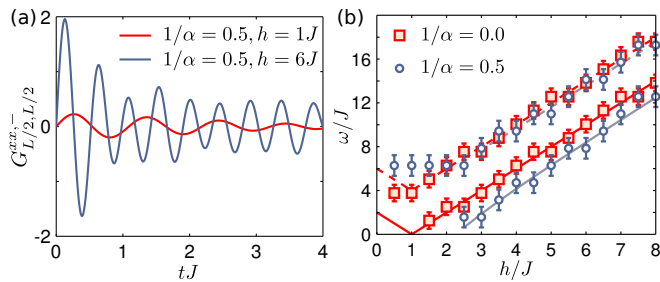


FIG. 4. (Color online) Dynamic Green's function  $G_{L/2,L/2}^{xx,-}(t)$  (a) of the long-range, transverse field Ising model (9) for interaction exponent  $\alpha = 2$  in the ferromagnetic ( $h = J$ ) and in the paramagnetic ( $h = 6J$ ) phase, see legend. (b) Oscillation frequencies, symbols, in  $G_{L/2,L/2}^{xx,-}(t)$  obtained from a Fourier transform of the time-dependent data as a function of the transverse field  $h$  for two different values of the interaction exponent  $\alpha$ . Error bars indicate the resolution of the Fourier transform in frequency space. Solid lines illustrates the excitation gap and dashed line the upper band edge, which define the oscillations contributing to the dynamic correlations.

coupling. Theoretically, quantum spin systems with long-range interactions that decay with arbitrary exponent  $\alpha$  have rarely been studied in the literature and so far static properties [26, 40–42] and quantum quenches [43–45] have been explored. This is why we discuss the one-dimensional, ferromagnetic ( $J > 0$ ), long-range, transverse-field Ising model in greater detail and focus in particular on dynamical correlation functions and on the quantum phase transition (QPT) from the ferromagnetic (FM) to the paramagnetic (PM) phase, whose universality is described by a continuous manifold of critical exponents that can be tuned by the decay of the interactions  $\alpha$ , see Fig. 3 (a) for the rich phase diagram.

The transverse field Ising model obeys the global symmetry  $\sigma^x \rightarrow -\sigma^x$ ,  $\sigma^y \rightarrow \sigma^y$  and  $\sigma^z \rightarrow -\sigma^z$  and thus only expectation values with an odd number of  $\sigma^x$  operators vanish in Eq. (5). However, when choosing the phases  $\phi_1 = 0$  and  $\phi_2 = \pi/2$  it can be shown that the many-body Ramsey protocol measures [12]

$$M_{ij}(0, \pi/2, t) = \frac{1}{2} G_{ij}^{xx,-}. \quad (10)$$

We illustrate that insight into the many-body physics can be obtained by studying systems which are currently experimentally realizable. To this end we solve systems of up to 22 ions with exact diagonalization based on the Lanczos technique [46] and calculate their dynamical Green's functions. As realized in experiments we generally consider open boundary conditions (OBC). In Fig. 4 (a) we show dynamic Green's functions  $G_{L/2,L/2}^{xx,-}$  for the interaction exponent  $\alpha = 2$  in the FM and in the PM phase. The time-resolved Green's functions characterize the many-body states: In the FM phase ( $h$  smaller than the critical field  $h_c$  that determines the QPT) the

response in the direction of the ferromagnet is small, which manifests in  $G_{L/2,L/2}^{xx,-}$  through small amplitude oscillations whose envelope decays very slowly, whereas in the PM phase ( $h > h_c$ ) the response is large, which in  $G_{L/2,L/2}^{xx,-}$  manifests in oscillations that initially have a large amplitude but decay quickly in time.

The oscillations in the dynamic Green's functions contain information about the excitations in the system. In particular, in the PM phase oscillations with a frequency corresponding to the gap [2] are expected. In addition, the spectrum is cut off due to the lattice, which gives rise to a second energy scale present in both the PM and the FM phase. In Fig. 4 (b) we show the frequency components extracted from the Fourier transform of  $G_{L/2,L/2}^{xx,-}(t)$  with error bars given by the resolution in frequency space for both short-ranged interactions ( $1/\alpha = 0$ , squares) and the long-ranged interactions ( $1/\alpha = 1/2$ , circles). For short-range interactions  $1/\alpha = 0$  the gap can be evaluated analytically  $\Delta = 2|h - J|$  [2], which grows linearly with the transverse field as indicated by the solid red (dark) line in Fig. 4 (b). The upper band edge at  $\Delta + 4J$  is indicated by the dashed red (dark) line. At the critical point  $h_c = J$  the gap closes, however oscillations from the finite bandwidth are still present. For long-ranged interactions, we extract the excitation gap and the bandwidth numerically. Results are shown by blue (light) solid and dashed lines, respectively. The upper band-edge, blue (light) dashed line, almost coincides with the short range system. The gap and the upper band-edge are in good agreement with the frequency components extracted from the correlation functions.

Along the quantum critical line  $h = h_c(\alpha)$ , which can be determined experimentally by measuring for example the Binder ratio [47], the system becomes scale invariant and thus spatial and temporal correlations decay as power laws (see Fig. 3 (b)). In [12] we show in detail that a change in the critical exponents should be observable in current experiments already with a medium number of ions.

**Conclusions and outlook.**—In summary, we proposed a protocol to measure real-space and time resolved spin correlation functions using many-body Ramsey interference. We discuss the protocol for two relevant examples of the Heisenberg and the long-range transverse field Ising model, which can be experimentally realized with cold atoms, polar molecules, and trapped ions. In this work we focused on spin-1/2 systems. However, the proposed protocol can be generalized to higher-spin systems when realizing the Rabi pulses (2) with the respective higher-spin operators. In order to implement the generalized spin-rotations, spin states should be encoded in internal atomic states with isotropic energy spacing which can be simultaneously addressed by Rabi pulses.

The measurement of the time dependent Green's functions provides important information on many-body ex-

citations and on quantum phase transitions where they exhibit specific scaling laws. Having such tools at hand makes it possible to explore fundamental, theoretically much debated many-body phenomena. In particular, we believe that the many-body localization transition [48–50] and many-body localized phases, which are characterized by a dephasing time that grows exponentially with the distance between two particles in the sample [51–53], can be explored using the ideas described in this work.

Another question is whether the many-body Ramsey protocol can be applied to systems out of equilibrium. The protocol we propose is based on discrete symmetries of many-body eigenstates and thus holds for ensembles described by diagonal density matrices, while a generic system out of equilibrium is characterized by a density matrix which also contains off-diagonal elements. However, if the off-diagonal elements dephase in time, many-body Ramsey interferometry can be applied out of equilibrium as well. This could for example also be the case for integrable systems which after fast dephasing are described by a diagonal density matrix whose weights are determined by the generalized Gibbs ensemble [54, 55].

**Acknowledgments.**—We thank S. Gopalakrishnan, R. Islam, C. Monroe, and S. Sachdev for useful discussions. The authors acknowledge support from Harvard-MIT CUA, the DARPA OLE program, AFOSR MURI on Ultracold Molecules, ARO-MURI on Atomtronics, the Austrian Science Fund (FWF) Project No. J 3361-N20, as well as the Swiss NSF under MaNEP and Division II. TG is grateful to the Harvard Physics Department and to Harvard-MIT CUA for support and hospitality during the completion of this work. Numerical calculations have been performed on the Odyssey cluster at Harvard University Research Computing.

---

\* [knap@physics.harvard.edu](mailto:knap@physics.harvard.edu)

- [1] A. L. Fetter and J. D. Walecka, *Quantum Theory of Many-Particle Systems* (McGraw-Hill, New York, 1971)
- [2] S. Sachdev, *Quantum Phase Transitions*, 2nd ed. (Cambridge University Press, Cambridge, UK, 2011)
- [3] I. Bloch, J. Dalibard, and W. Zwerger, *Rev. Mod. Phys.* **80**, 885 (2008)
- [4] T. Lahaye, C. Menotti, L. Santos, M. Lewenstein, and T. Pfau, *Rep. Prog. Phys.* **72**, 126401 (2009)
- [5] R. Blatt and C. F. Roos, *Nat. Phys.* **8**, 277 (2012)
- [6] C. Kollath, A. Iucci, T. Giamarchi, W. Hofstetter, and U. Schollwöck, *Phys. Rev. Lett.* **97**, 050402 (2006)
- [7] A. Tokuno and T. Giamarchi, *Phys. Rev. Lett.* **106**, 205301 (2011)
- [8] M. Endres, T. Fukuhara, D. Pekker, M. Cheneau, P. Schauß, C. Gross, E. Demler, S. Kuhr, and I. Bloch, *Nature* **487**, 454 (2012)
- [9] J. T. Stewart, J. P. Gaebler, and D. S. Jin, *Nature* **454**, 744 (2008)
- [10] M. A. Nielsen and I. L. Chuang, *Quantum Computation and Quantum Information* (Cambridge University Press, Cambridge, UK, 2000)
- [11] H. Häffner, C. Roos, and R. Blatt, *Phys. Rep.* **469**, 155 (2008)
- [12] See supplementary material
- [13] A. M. Rey, V. Gritsev, I. Bloch, E. Demler, and M. D. Lukin, *Phys. Rev. Lett.* **99**, 140601 (2007)
- [14] S. Trotzky, P. Cheinet, S. Fölling, M. Feld, U. Schnorrberger, A. M. Rey, A. Polkovnikov, E. A. Demler, M. D. Lukin, and I. Bloch, *Science* **319**, 295 (2008)
- [15] S. Nascimbène, Y.-A. Chen, M. Atala, M. Aidelsburger, S. Trotzky, B. Paredes, and I. Bloch, *Phys. Rev. Lett.* **108**, 205301 (2012)
- [16] T. Fukuhara, A. Kantian, M. Endres, M. Cheneau, P. Schauß, S. Hild, D. Bellem, U. Schollwöck, T. Giamarchi, C. Gross, I. Bloch, and S. Kuhr, *Nat. Phys.* **9**, 235 (2013)
- [17] D. Greif, T. Uehlinger, G. Jotzu, L. Tarruell, and T. Esslinger, *Science* **340**, 1307 (2013)
- [18] The short-range, transverse field Ising model [56] as well as frustrated classical magnetism [57] have also been explored with cold atoms.
- [19] A. V. Gorshkov, S. R. Manmana, G. Chen, J. Ye, E. Demler, M. D. Lukin, and A. M. Rey, *Phys. Rev. Lett.* **107**, 115301 (2011)
- [20] A. V. Gorshkov, S. R. Manmana, G. Chen, E. Demler, M. D. Lukin, and A. M. Rey, *Phys. Rev. A* **84**, 033619 (2011)
- [21] B. Yan, S. A. Moses, B. Gadway, J. P. Covey, K. R. A. Hazzard, A. M. Rey, D. S. Jin, and J. Ye, *Nature (London)* **501**, 521 (2013)
- [22] D. P. Arovas and A. Auerbach, *Phys. Rev. B* **38**, 316 (1988)
- [23] A. Auerbach and D. P. Arovas, *Phys. Rev. Lett.* **61**, 617 (1988)
- [24] A. Auerbach, *Interacting electrons and quantum magnetism* (Springer, New York, 1994)
- [25] E. Manousakis, *Rev. Mod. Phys.* **63**, 1 (1991)
- [26] A. Dutta and J. K. Bhattacharjee, *Phys. Rev. B* **64**, 184106 (2001)
- [27] E. Luijten and H. Meßingfeld, *Phys. Rev. Lett.* **86**, 5305 (2001)
- [28] A. W. Sandvik, *Phys. Rev. E* **68**, 056701 (2003)
- [29] D. Porras and J. I. Cirac, *Phys. Rev. Lett.* **92**, 207901 (2004)
- [30] X.-L. Deng, D. Porras, and J. I. Cirac, *Phys. Rev. A* **72**, 063407 (2005)
- [31] A. Friedenauer, H. Schmitz, J. T. Glueckert, D. Porras, and T. Schaetz, *Nat. Phys.* **4**, 757 (2008)
- [32] R. Islam, E. Edwards, K. Kim, S. Korenblit, C. Noh, H. Carmichael, G.-D. Lin, L.-M. Duan, C.-C. Joseph Wang, J. Freericks, and C. Monroe, *Nat. Commun.* **2**, 377 (2011)
- [33] K. Kim, M.-S. Chang, R. Islam, S. Korenblit, L.-M. Duan, and C. Monroe, *Phys. Rev. Lett.* **103**, 120502 (2009)
- [34] K. Kim, M.-S. Chang, S. Korenblit, R. Islam, E. E. Edwards, J. K. Freericks, G.-D. Lin, L.-M. Duan, and C. Monroe, *Nature* **465**, 590 (2010)
- [35] E. E. Edwards, S. Korenblit, K. Kim, R. Islam, M.-S. Chang, J. K. Freericks, G.-D. Lin, L.-M. Duan, and C. Monroe, *Phys. Rev. B* **82**, 060412(R) (2010)
- [36] B. P. Lanyon, C. Hempel, D. Nigg, M. Müller, R. Gerritsma, F. Zähringer, P. Schindler, J. T. Barreiro, M. Rambach, G. Kirchmair, M. Hennrich, P. Zoller,

- R. Blatt, and C. F. Roos, *Science* **334**, 57 (2011)
- [37] J. W. Britton, B. C. Sawyer, A. C. Keith, C.-C. J. Wang, J. K. Freericks, H. Uys, M. J. Biercuk, and J. J. Bollinger, *Nature* **484**, 489 (2012)
- [38] R. Islam, C. Senko, W. C. Campbell, S. Korenblit, J. Smith, A. Lee, E. E. Edwards, C.-C. J. Wang, J. K. Freericks, and C. Monroe, *Science* **340**, 583 (2013)
- [39] P. Richerme, C. Senko, S. Korenblit, J. Smith, A. Lee, R. Islam, W. C. Campbell, and C. Monroe, *Phys. Rev. Lett.* **111**, 100506 (2013)
- [40] N. Laflorencie, I. Affleck, and M. Berciu, *J. Stat. Mech.* **2005**, P12001 (2005)
- [41] A. W. Sandvik, *Phys. Rev. Lett.* **104**, 137204 (2010)
- [42] T. Koffel, M. Lewenstein, and L. Tagliacozzo, *Phys. Rev. Lett.* **109**, 267203 (2012)
- [43] M. L. Wall and L. D. Carr, *New J. Phys.* **14**, 125015 (2012)
- [44] P. Hauke and L. Tagliacozzo, arXiv:1304.7725
- [45] J. Schachenmayer, B. P. Lanyon, C. F. Roos, and A. J. Daley, *Phys. Rev. X* **3**, 031015 (2013)
- [46] Y. Saad, *Numerical Methods for Large Eigenvalue Problems* (Manchester University Press, 1995)
- [47] K. Binder, *Phys. Rev. Lett.* **47**, 693 (1981)
- [48] D. Basko, I. Aleiner, and B. Altshuler, *Ann. Phys.* **321**, 1126 (2006)
- [49] I. V. Gornyi, A. D. Mirlin, and D. G. Polyakov, *Phys. Rev. Lett.* **95**, 206603 (2005)
- [50] V. Oganesyan and D. A. Huse, *Phys. Rev. B* **75**, 155111 (2007)
- [51] M. Serbyn, Z. Papić, and D. A. Abanin, *Phys. Rev. Lett.* **110**, 260601 (2013)
- [52] D. A. Huse and V. Oganesyan, arXiv:1305.4915
- [53] M. Serbyn, Z. Papić, and D. A. Abanin, *Phys. Rev. Lett.* **111**, 127201 (2013)
- [54] M. Rigol, V. Dunjko, V. Yurovsky, and M. Olshanii, *Phys. Rev. Lett.* **98**, 050405 (2007)
- [55] M. Rigol, V. Dunjko, and M. Olshanii, *Nature* **452**, 854 (2008)
- [56] J. Simon, W. S. Bakr, R. Ma, M. E. Tai, P. M. Preiss, and M. Greiner, *Nature* **472**, 307 (2011)
- [57] J. Struck, C. Ölschläger, R. L. Targat, P. Soltan-Panahi, A. Eckardt, M. Lewenstein, P. Windpassinger, and K. Sengstock, *Science* **333**, 996 (2011)
- [58] D. J. Thouless, *Phys. Rev.* **187**, 732 (1969)
- [59] J. M. Kosterlitz, *Phys. Rev. Lett.* **37**, 1577 (1976)
- [60] J. L. Cardy, *J. Phys. A: Math. Gen.* **14**, 1407 (1981)
- [61] J. Bhattacharjee, S. Chakravarty, J. L. Richardson, and D. J. Scalapino, *Phys. Rev. B* **24**, 3862 (1981)
- [62] J. Jaklič and P. Prelovšek, *Phys. Rev. B* **49**, 5065 (1994)
- [63] M. Aichhorn, M. Daghofer, H. G. Evertz, and W. von der Linden, *Phys. Rev. B* **67**, 161103(R) (2003)

### Technical details on many-body Ramsey interferometry

We present the calculation of the full expectation value (3), including the odd terms of spin operators, which is measured with many-body Ramsey interferometry. To

this end we introduce

$$\begin{aligned}\hat{C}(t) &:= e^{i\hat{H}t} R^\dagger(\phi_2) \sigma_j^z R(\phi_2) e^{-i\hat{H}t} \\ &= -[\sigma_j^x(t) \sin \phi_2 + \sigma_j^y(t) \cos \phi_2].\end{aligned}$$

With that we obtain

$$\begin{aligned}M_{ij} &= \frac{1}{2} \langle i[\hat{C}(t), \sigma_i^x] \cos \phi_1 - i[\hat{C}(t), \sigma_i^y] \sin \phi_1 + \hat{C}(t) \\ &\quad + (\sigma_i^x \cos \phi_1 - \sigma_i^y \sin \phi_1) \hat{C}(t) (\sigma_i^x \cos \phi_1 - \sigma_i^y \sin \phi_1) \rangle.\end{aligned}$$

The commutators of  $\hat{C}(t)$  with the spin operators  $\sigma_i^{x,y}$  yield the Green's functions, whereas the other terms contain either one or three spin operators.

As discussed in the main text, the expectation value of odd numbers of spin operators vanishes trivially for the Heisenberg model. For the long-ranged, transverse field Ising model they vanish provided

$$\cos \phi_2 = 0 \quad \text{and} \quad \sin \phi_1 \cos \phi_1 = 0,$$

which is fulfilled when locking the phases of the laser field to  $\phi_2 = \pi/2$  and  $\phi_1 = \{0, \pi/2\}$ . For the latter choice of the phase  $\phi_1 = \pi/2$  the whole expression (3) vanishes, whereas for  $\phi_1 = 0$  it gives Eq. (10).

### Spin-shelving protocol

Projecting one spin state onto an auxiliary level, allows one to extract the anticommutator, Green's function  $G_{ij}^{zz,+}$  in the orthogonal spin direction compared to the Green's functions accessible via many-body Ramsey interference. The protocol is as follows: First, a transition between one state of the two level system, say  $|\downarrow\rangle_z$ , and an auxiliary level  $|a\rangle$  has to be driven strongly, see Fig. 5 for the level scheme. The state  $|a\rangle$  should decay spontaneously into a metastable state  $|b\rangle$ . This process shelves the  $|\downarrow\rangle_z$  state to the auxiliary level  $|b\rangle$ , which might give rise to a complicated time evolution. However, the protocol includes disregarding all experimental runs where auxiliary level  $|b\rangle$  is populated at the end of the time evolution. Following that protocol a spin projection operator of the form  $\hat{P}_i = (\hat{1} + \sigma_i^z)/2$  is realized which allows one to extract the anticommutator Green's function

$$\langle \hat{P}_i^\dagger e^{i\hat{H}t} \sigma_j^z e^{-i\hat{H}t} \hat{P}_i \rangle = iG_{ij}^{zz,+} + \text{terms with one } \sigma^z. \quad (11)$$

The experimental challenge of the protocol is that instead of two states, three states have to be detected.

For the Heisenberg model (6), the spin-shelving technique measures  $G_{ij}^{zz,+}$  in the case of zero magnetization  $m_z = \sum_r \sigma_r^z = 0$ , where the ground state has the additional global symmetry  $\sigma^x \rightarrow -\sigma^x$ ,  $\sigma^y \rightarrow \sigma^y$  and  $\sigma^z \rightarrow -\sigma^z$  and thus expectation values with odd numbers of spin-z operators vanish.

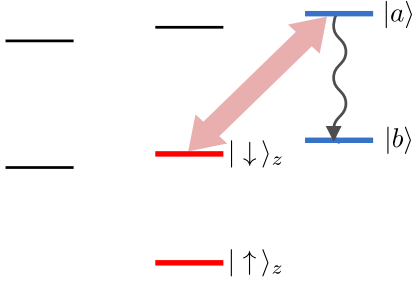


FIG. 5. (Color online) Level scheme required for the spin-shelving protocol. The thick red arrow illustrates the strong drive between  $|\downarrow\rangle_z$  and an auxiliary level  $|a\rangle$ , which decays spontaneously to a metastable state  $|b\rangle$ , as indicated by the black wavy arrow (see text for details).

In the case of the long-range, transverse field Ising model (9) that global symmetry is trivially fulfilled. Thus the spin-shelving technique allows one to measure  $G_{ij}^{zz,+}$ , which is further related to  $G_{ij}^{xx,+}(t)$  through

$$G_{ij}^{zz,\mp}(t) = -\frac{1}{4\hbar^2} \frac{d^2}{dt^2} G_{ij}^{xx,\mp}(t), \quad (12)$$

as commuting  $\hat{H}_{\text{Ising}}$  with  $\sigma_i^x$  generates  $\sigma_i^z$ . Hence, for the long-ranged, transverse field Ising model (9) the spin-shelving technique also makes it possible to explore  $G_{ij}^{xx,+}(t)$ .

### Loschmidt echo

The Loschmidt echo is defined as

$$\mathcal{L}(t) := \frac{1}{Z} \sum_n e^{-\beta E_n} \langle n | e^{i\hat{H}_0 t} e^{-i\hat{H}_1 t} | n \rangle,$$

which describes a forward propagation in time with Hamiltonian  $\hat{H}_1 := \hat{H}_0 + \hat{V}$  and a backward propaga-

tion with  $\hat{H}_0$  for the same time period. In the following, we assume that  $\hat{V}$  is a local perturbation. We expect that if the system is in a localized regime, a local perturbation does not have a dramatic effect and eigenstates of  $\hat{H}_0 + \hat{V}$  and  $\hat{H}_0$  differ only slightly. Hence  $\mathcal{L}(t)$  will oscillate in time without fully decaying. By contrast, if the system is in a diffusive regime,  $\mathcal{L}(t)$  should decay quickly in time.

It is useful to point out that Green's functions which are local in space are directly connected to the Loschmidt echo

$$\begin{aligned} G_{jj}^{aa,\mp} &= -i\theta(t) \langle \sigma_j^a(t) \sigma_j^a(0) \mp \sigma_j^a(0) \sigma_j^a(t) \rangle \\ &= -i\theta(t) \langle \underbrace{e^{i\hat{H}t} \sigma_j^a e^{-i\hat{H}t} \sigma_j^a \mp \sigma_j^a e^{i\hat{H}t} \sigma_j^a e^{-i\hat{H}t}}_{:=e^{i\hat{H}_1 t}} \rangle \\ &= -i\theta(t) [\mathcal{L}(t) \mp \mathcal{L}(-t)] \end{aligned}$$

with  $\hat{H}_0 = \hat{H}$  and  $\hat{H}_1$  is identical to  $\hat{H}$  except for the local spin transformation:  $\sigma_j^a \rightarrow \sigma_j^a$  and  $\sigma_j^b \rightarrow -\sigma_j^b$ , for  $b \neq a$ .

From these considerations immediately follows that the proposed many-body Ramsey interference and the spin-shelving technique can be used to distinguish localized and diffusive phases.

### Spin-echo protocol

An external magnetic field, which slowly changes between individual experimental runs, couples to the system in form of a Zeeman term

$$\hat{H}_Z = h_z \sum_i \sigma_i^z. \quad (13)$$

Here we discuss under which requirements spin echo can be used to remove these fluctuations. The spin-echo protocol differs from the many-body Ramsey protocol by a global  $\pi$  rotation  $R_\pi := R(\pi, \phi_\pi)$  performed at time  $t/2$

$$\tilde{M}_{ij}(\phi_1, \phi_2, t) = \sum_n \frac{e^{-\beta E_n}}{Z} \langle n | R_i^\dagger(\phi_1) e^{i\hat{H}t/2} R_\pi^\dagger e^{i\hat{H}t/2} R^\dagger(\phi_2) \sigma_j^z R(\phi_2) e^{-i\hat{H}t/2} R_\pi e^{-i\hat{H}t/2} R_i(\phi_1) | n \rangle. \quad (14)$$

The rotation  $R_\pi$ , see Eq. (2), explicitly reads

$$R_\pi = \prod_j i(\sigma_j^x \cos \phi_\pi - \sigma_j^y \sin \phi_\pi).$$

It transforms the spins of the Hamiltonian as follows:

$$\forall \text{ sites: } \sigma^a \rightarrow \sigma^a, \sigma^b \rightarrow -\sigma^b, \text{ for } a \neq b. \quad (15)$$

Using the fact that  $a \in \{x, y\}$  the sign of  $\sigma^z$  is always flipped under that transformation. Thus the Zeeman field Eq. (13) in  $z$ -direction is canceled, as from 0 to  $t/2$   $\hat{H}_Z$  evolves with positive sign, whereas the from  $t/2$  to  $t$  its evolution enters with negative sign, provided the Hamiltonian commutes with  $\hat{H}_Z$ , see also Eq. (8).

The Heisenberg model (6) fulfills these requirements and thus Zeeman field fluctuations can be removed using the spin-echo protocol. A detailed calculation shows that

$$\begin{aligned} \tilde{M}_{ij}(\phi_1, \phi_2, t) = & \frac{1}{4} \cos 2\phi_\pi \{ \sin(\phi_1 + \phi_2)(G_{ij}^{xx} + G_{ij}^{yy}) - \cos(\phi_1 + \phi_2)(G_{ij}^{xy} - G_{ij}^{yx}) \} \\ & - \frac{1}{4} \sin 2\phi_\pi \{ \cos(\phi_1 + \phi_2)(G_{ij}^{xx} + G_{ij}^{yy}) - \sin(\phi_1 + \phi_2)(G_{ij}^{xy} - G_{ij}^{yx}) \}. \end{aligned} \quad (16)$$

For the choice of  $\phi_\pi = 0$  or  $\phi_\pi = \pi/2$  only the first line of Eq. (16) contributes and corresponds to the many-body Ramsey interference (7) with  $\phi_2 \rightarrow -\phi_2$ .

The long-range, transverse field Ising model (9), is only invariant under (15) if  $a = y$ , i.e.,  $\phi_\pi = \pi/2$ . As for many-body Ramsey interference, the phases  $\phi_1$  and  $\phi_2$  have to be chosen such that the odd number of  $\sigma^{x,y}$  operators vanish. This can be achieved again with  $\phi_1 = 0$  and  $\phi_2 = \pi/2$  where we find

$$\tilde{M}_{ij}(0, \pi/2, t) = -\frac{1}{2} G_{ij}^{xx}. \quad (17)$$

However, the Zeeman term does not commute with the Ising Hamiltonian. Thus the evolution of both contributions is entangled and cannot be undone with spin-echo. Using the Baker-Campbell-Hausdorff formula, it can be shown that the dynamic is governed by the Ising Hamiltonian to order  $O(t^2 h_z)$ , i.e., for short times and small changes in the magnetic field. However, for current experimental realizations with trapped  $^{171}\text{Yb}^+$  ions it is not necessary to aim at a spin-echo procedure, as the hyperfine-states which are used to encode the spin states do not couple to the Zeeman field.

### Dynamic signature of long-range order in the Heisenberg antiferromagnet

In the two-dimensional Heisenberg antiferromagnet long-range order occurs only at zero temperature. However, even at non-zero temperatures the dynamic structure factor contains signatures of the long-range order when evaluated at the antiferromagnetic ordering wave-vector  $\mathbf{q} = \vec{\pi}$ . The dynamic structure factor is defined as

$$S_{\mathbf{q}}^\alpha(t) := \sum_{\mathbf{r}} e^{-i\mathbf{q}\mathbf{r}} \langle \sigma_{\mathbf{r}}^\alpha(t) \sigma_{\mathbf{0}}^\alpha \rangle. \quad (18)$$

and can thus be evaluated from the spatially resolved Ramsey experiments when adding up contributions from one sublattice with positive sign and the other with negative sign.

Typically, in condensed matter experiments, the dynamic structure factor is measured as a function of frequency  $S_{\mathbf{q}}^\alpha(\omega)$ , which is related to  $S_{\mathbf{q}}^\alpha(t)$  through Fourier transformation. A signature of long-range order in  $S_{\vec{\pi}}^\alpha(\omega)$  is mode softening and accumulation of the zero energy peak with decreasing temperature. This is demonstrated

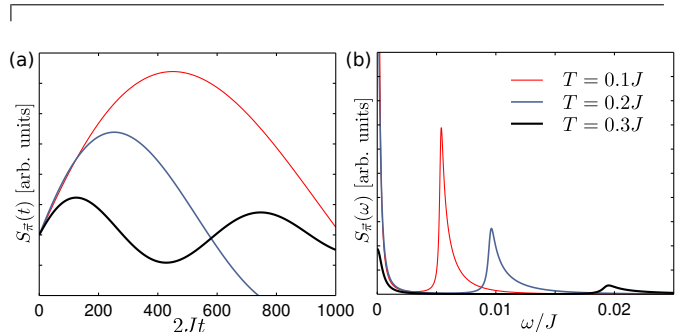


FIG. 6. (Color online) Time dependent (a) and frequency resolved (b) structure factor at the antiferromagnetic ordering wave-vector  $\vec{\pi}$  evaluated at different temperatures, see legend. The built up of antiferromagnetic correlations manifests in the strong increase of the period and the amplitude of the oscillations in the time dependent structure factor.

in Fig. 6 (b). In the time resolved measurement the absence of antiferromagnetic order would manifest in fast, small-amplitude oscillations of  $S_{\vec{\pi}}(t)$ , whereas the onset of long-range order manifests in a dramatic increase of the amplitude and period of the oscillations, as with decreasing temperature smaller energy scales are involved, Fig. 6 (a).

### Quantum phase transition of the ferromagnetic, long-range, transverse field Ising model

In Fig. 3 (a) we show the phase of the one-dimensional, ferromagnetic, long-range, transverse field Ising model diagram in the transverse field  $h$ , interaction exponent  $\alpha$ , and temperature  $T$  space, which exhibits particularly rich physics. For  $\alpha < 1$  the system is thermodynamically unstable as the energy per site diverges, hatched region. Starting out with a Ginzburg-Landau action, we summarize the main properties of the zero temperature phase transition (see also [26])

$$S = \frac{1}{2} \int \frac{d\omega}{2\pi} \int \frac{dk}{2\pi} (\omega^2 + ck^2 + r + V(k)) \phi_k^2 + \frac{u}{4!} S_u \quad (19)$$

where  $S_u$  contains the  $\phi^4$  term and  $V(k)$  is the Fourier transform of the long-range interactions which scales as  $\sim k^{\alpha-1}$ . Thus  $V(k)$  renormalizes to zero for  $\alpha \geq 3$



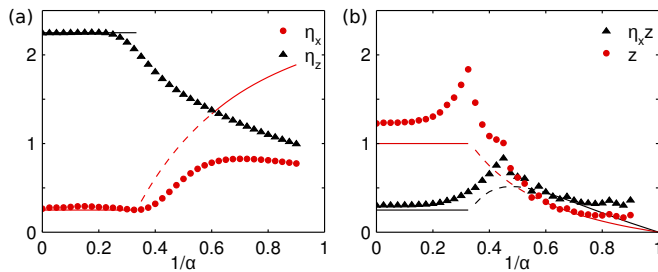


FIG. 7. (Color online) (a) Critical exponent  $\eta_x$  ( $\eta_z$ ), symbols, extracted from the extrapolation of finite size data of the spatial correlations along the quantum critical line and (b) critical exponent  $\eta_x z$  of dynamic correlations  $G_{L/2, L/2}^{xx, -}(t)$  and dynamical exponent  $z$ , symbols. As a function of the interaction exponent  $\alpha$  the quantum phase transition follows a continuous manifold of universality classes characterized by a set of continuously changing critical exponents. Solid lines are exact results for the critical exponents in the thermodynamic limit, and the dashed lines are extrapolations.

and the phase transition is of the universality class of the short-range Ising transition, dark gray region. For  $\alpha < 3$  the free propagator is of the form  $G_{(0)}^{xx}(k, \omega) \sim (\omega^2 + r + vk^{\alpha-1})^{-1}$ . From the temporal and the spatial correlations along the critical line, the dynamical critical exponent  $z(\alpha)$ , which relates the scaling of space and time

$$t \sim r^{z(\alpha)} \quad (20)$$

can be extracted.  $z(\alpha)$  is a continuous function of the interaction exponent  $\alpha$ . From the free propagator we find at the critical point  $r = 0$  the mean-field dynamical critical exponent  $z^{\text{mf}} = (\alpha - 1)/2$ , and spatial critical exponent  $\eta_x^{\text{mf}} = 3 - \alpha$ . Instead of an upper critical dimension, we can now talk about a lower critical interaction exponent  $\alpha_l$  below which mean-field becomes exact. Power counting and applying the condition that the scaling dimension of the coefficient  $u$  of the  $\phi^4$  term [ $S_u$  in Eq. (19)] vanishes, gives  $\alpha_l = 5/3$ . For interactions which decay

slower, as indicated by the light gray region, mean-field exponents are valid.

At zero temperature we extracted the critical point from extrapolating the maxima of the von Neumann entropy, which in the thermodynamic limit should diverge at the transition, for systems up to 22 ions and periodic boundary conditions. Experimentally, the location of the quantum phase transition can be obtained for example from the Binder ratio [47].

On the ferromagnetic side there is a finite temperature transition for  $\alpha < 2$ . For faster decay there is a crossover [2]. At  $\alpha = 2$  and  $h = 0$ , dashed lines, a Berezinskii-Kosterlitz-Thouless (BKT) transition occurs [58–61], as the energy for a domain wall diverges logarithmically. The BKT transition also extends to finite transverse field  $h$  [26]. The symbols showing the finite temperature transition for  $h = 0$  ( $h = J/2$ ) are (quantum) Monte-Carlo results [27, 28]. We also calculate the location of the phase transition using finite temperature Lanczos techniques [62, 63], which lead to an agreement to the quantum Monte-Carlo within 10%.

Critical exponents for spatial correlations extrapolated for systems with OBC up to  $L = 20$  are shown in Fig. 7 (a), symbols. For the short-ranged, transverse field Ising model it is well known that the Fisher exponent  $\eta_x = 1/4$ , the critical exponent  $z = 1$  and thus we can deduce from Eq. (12)  $\eta_z = 9/4$ , which we recover well within our finite size extrapolations. For slowly decaying interactions the system sizes are too small to recover the exact exponents, but a pronounced change in the critical exponents when crossing over  $\alpha = 3$  can be observed. Exactly known values for the exponents are indicated by solid lines, whereas dashed lines are extrapolations between the Ising and the mean field limit. Critical dynamic exponents  $\eta_x z$  for  $G_{L/2, L/2}^{xx, -}(t)$  are shown in Fig. 7 (b), as well as the dynamical exponent  $z$  obtained from the ratio of the dynamic and the spatial correlations, symbols. They agree reasonably with the exact results ( $\alpha > 3$  and  $\alpha < 5/3$ ) even though the systems available to extrapolate are rather small.